Deng et al. *Quantum Frontiers* (2026) 5:2
https://doi.org/10.1007/s44214-026-00100-3

Quantum Frontiers

ORIGINAL ARTICLE

Open Access

Valley-polarized Josephson junctions as gate-tunable 0-π qubit platforms

Yu-Xuan Deng[1†], Zhong C.F. Li[1†], Zi-Ting Sun[1], Jin-Xin Hu[1] and K.T. Law[1*]

Abstract

Recently, gate-defined Josephson junctions based on magic-angle twisted bilayer graphene (MATBG) have been fabricated. In such a junction, local electrostatic gating can create two superconducting regions connected by an interaction-driven valley-polarized state as the weak link. Due to the spontaneous time-reversal and inversion symmetry breaking, novel phenomena such as the Josephson diode effect have been observed with zero external magnetic fields. Importantly, when the so-called nonreciprocity efficiency (which measures the sign and strength of the Josephson diode effect) changes sign, the energy-phase relation of the junction is approximately $F(\phi) \propto \cos(2\phi)$ where F is the free energy and ϕ is the phase difference of the two superconductors. In this work, we show that such a MATBG-based Josephson junction, when shunted by a capacitor, can be used to realize the long-sought-after 0-π qubits which are protected from local perturbation-induced decoherence. Interestingly, by changing the junction parameters to the regime where a large nonreciprocity efficiency is obtainable, transmon-like qubits with large anharmonicity can also be realized. The gate-defined Josephson junctions can be employed as platforms for realizing qubits that are protected from local perturbations.

Keywords: Superconducting qubit, Josephson junction, Magic angle twisted bilayer graphene, Josephson diode effect

1 Introduction

Superconducting circuits provide versatile platforms for exploring quantum physics [1–3] and quantum information processing [4–9]. In these circuits, two energy levels, such as the ground state and the first excited state, can serve as qubit states for encoding quantum information, provided that the two states can be reliably distinguished and selectively controlled [10, 11]. The crucial components in these circuits are Josephson junctions [12], which can introduce isolated and controllable energy levels through large nonlinearity [13].

Currently, there are several promising superconducting qubit platforms with their own strengths and limitations. For example, a charge qubit [14–17] can be constructed using a single Josephson junction shunted by a capacitor with small capacitance. In this case, the Josephson junction has a large anharmonicity but is sensitive to charge noise. Another qubit architecture is transmon which is a Josephson junction coupled to a capacitor with large capacitance [17–19]. A transmon qubit is robust against charge noise at the expense of a smaller anharmonicity of energy levels. On the other hand, flux qubits [20–23] are built from a superconducting loop which contains a series of Josephson junctions and penetrated by an external magnetic flux. The energy levels are charge-insensitive and have large anharmonicity. However, the fluctuations of the magnetic flux introduce additional decoherence. To overcome decoherence, 0-π qubits with two degenerate ground states [24–28] as the qubit states were proposed, in which the qubits are protected from local-noise decoherence as pointed out by Kitaev [24]. However, even with

*Correspondence: phlaw@ust.hk
[1]Department of Physics, Hong Kong University of Science and Technology, Clear Water Bay, Hong Kong SAR, China
†Equal contributors

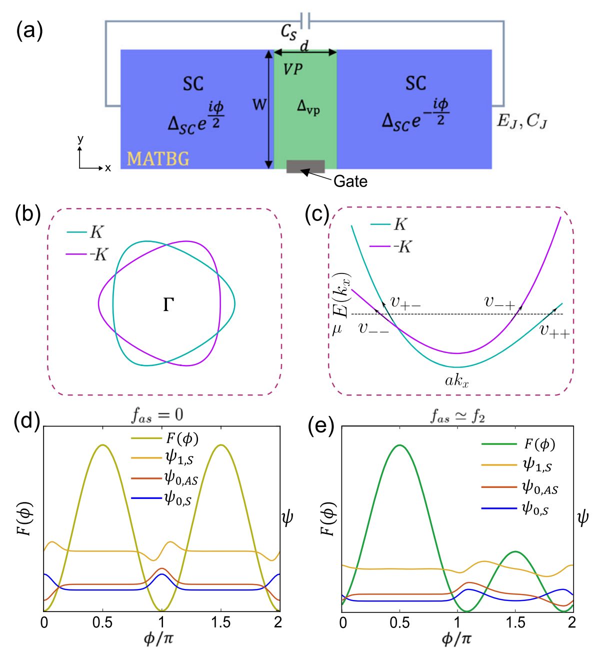

Figure 1 (a) A schematic picture of valley-polarized Josephson qubit. The central weak link is valley-polarized (VP) with the order parameter $\Delta_{\rm vp}$, while the left and right regions are superconductors (SC) with pairing potential $\Delta_{\rm sc}$. (b) The trigonally warped Fermi surface from Eq. (2). (c) Band dispersion of the $k_y = 0$ channel, with the black arrows indicating the Fermi velocity $v_{\tau,\alpha}$. Here, $\tau = \pm$ denotes the $\pm K$ valleys and $\alpha = \pm$ labels the left and right movers of electrons, respectively. (d)-(e) The schematic energy-phase relations and the amplitude of the eigenstates of the junction for two different parameter regimes. The left y-axis is the Josephson free energy $F(\phi)$, and $\psi_{0,S}$, $\psi_{0,AS}$ and $\psi_{1,S}$ denote the symmetric and antisymmetric qubit states and the third energy level, respectively. The energy-phase relations in (d) and (e) resemble those of 0-π qubits and flux qubits respectively

some experimental success, the realization of 0-π qubits is hindered by the complexity of the circuit design [29].

In this Letter, we point out that recent experimental advancements in fabricating gate-defined Josephson junctions based on magic-angle twisted bilayer graphene (MATBG) have opened a novel pathway for engineering highly gate-tunable 0-π qubits. In the MATBG-based Josephson junction [30], electrostatic gating can define two superconducting regions which are connected by a valley-polarized, time-reversal symmetry breaking weak link region [30–32]. The valley-polarized state [33] is an important state of matter in which the degeneracy of the states from the K and $-K$ valleys are lifted by electron-electron interactions [as schematically shown in Fig. 1 (c)]. Importantly, the valley-polarized state gives rise to unconventional phenomena such as the creation of the ϕ_0-Josephson junctions [31] and the Josephson diode effect [32]. The key message here is that the MATBG-based, gate-defined Josephson junction can be a new platform for engineering 0-π qubits which are immune to charge noise and phase fluctuations, and no magnetic flux is needed as time-reversal is broken spontaneously. Importantly, the Josephson diode effect [34–47] can be used to detect the parameter regimes of the qubit.

To describe the diode effect in the gate-defined Josephson junction based on MATBG [30], we previously demonstrated that the unconventional energy-phase relation $F(\phi)$ of the junction takes the form [32]

$$F(\phi) = f_{\rm vp}\cos\phi + f_{\rm as}\sin\phi + f_2\cos 2\phi. \tag{1}$$

Here, $f_{\rm vp}$ denotes the first harmonic term that can be modulated by valley polarization through electrostatic gating, $f_{\rm as}$ is the asymmetric term from intra-valley inversion symmetry breaking which is also gate-tunable, whereas f_2 is the second harmonic term. Importantly, the parameters of the Josephson energy can be gate-tuned to be dominated by the $\cos 2\phi$ term when $f_{\rm vp} = f_{\rm as} = 0$. This happens when the diode efficiency changes sign [32] which can be measured experimentally. Importantly, when such a Josephson junction is shunted by a capacitor, a 0-π qubit or transmon qubit is obtained as schematically shown in Fig. 1 (a). The energy-phase relations in the 0-π qubit and the transmon qubit regimes are schematically shown in Fig. 1 (d) and (e), respectively. The advantage of the setup in Fig. 1 (a) is that a 0-π qubit can be realized by a single Josephson junction without sophisticated circuit design [24–27].

2 Methods

2.1 Model of gate-defined Josephson junction in MATBG

The low energy effective Hamiltonian of the MATBG in the moiré Brillouin zone can be described by [31–33]

$$H_{0,\tau}(\mathbf{k}) = \lambda_0(k_x^2 + k_y^2) + \tau\lambda_1 k_x(k_x^2 - 3k_y^2) - \mu, \tag{2}$$

where $\tau = \pm$ is the valley index, μ is the Fermi energy, λ_0 is a constant parameterizing the band dispersion and λ_1 is the trigonal warping strength which breaks the intravalley inversion symmetry and is essential for the Josephson diode effect [32]. The trigonally warped Fermi surface is depicted in Fig. 1 (b).

For the 2D Josephson junction shown in Fig. 1 (a), we assume the periodic boundary condition along the y-direction and for each k_y near the Fermi surface, the normal state Hamiltonian can be linearized as $H_{0,\tau\alpha}(x,k_y) = -i\alpha\hbar v_{f,\tau\alpha}(x,k_y)\partial_x$, where $\alpha = \pm$ labels the sign of the Fermi velocity for left-moving and right-moving electrons, respectively. The Fermi velocity can be written as $v_{f,\tau\alpha}(x,k_y) = v_{{\rm vp},\tau\alpha}(x,k_y)\Theta(x)\Theta(d-x) + v_{{\rm sc},\tau\alpha}(x,k_y)[\Theta(-x) + \Theta(x-d)]$, including both the valley-polarized and the superconducting regions. The intravalley inversion symmetry breaking indicates the fact that $v_{f,\tau\alpha} \neq v_{f,\tau\bar{\alpha}}$ [Fig. 1 (c)]. For brevity, $\bar{\tau}$ and $\bar{\alpha}$ are used to denote $-\tau$ and $-\alpha$, respectively. In the following, $k_y = 0$ is assumed for analytical calculations. The results for the two-dimensional case will be given by a lattice model calculation later. Additionally, it is assumed that the spin degrees of freedom are degenerate, so the spin index is omitted. To describe the whole Josephson junction with superconducting regions, we define $\psi_{\tau\alpha}(x)$ ($\psi^{\dagger}_{\tau\alpha}(x)$) to be the annihilation (creation) operator for an electron at τ valley with Fermi velocity in the α direction. In the Nambu basis $[\psi_{\tau\alpha}(x), \psi^{\dagger}_{\bar{\tau}\bar{\alpha}}(x)]^T$, the linearized Bogoliubov-de Gennes (BdG) Hamiltonian of the Josephson junction is

$$H_{\tau\alpha}(x) = \begin{pmatrix} H_{0,\tau\alpha}(x) + \Delta_{\rm vp}(x) & \Delta_{\rm sc}(x) \\ \Delta^*_{\rm sc}(x) & -H^*_{0,\bar{\tau}\bar{\alpha}}(x) + \Delta_{\rm vp}(x) \end{pmatrix}, \quad (3)$$

where $\Delta_{\rm vp}(x) = \tau\Delta_{\rm vp}\Theta(x)\Theta(d-x)$ is the valley polarization order parameter, and $\Delta_{\rm sc}(x) = \Delta_{\rm sc}[e^{i\frac{\phi}{2}}\Theta(-x) + e^{-i\frac{\phi}{2}}\Theta(x-d)]$ is the superconducting pairing order parameter [Fig. 1 (a)]. From Eq. (3), the energy-phase relation can be calculated analytically using the scattering matrix method [48–51], which reads

$$F(\phi) = -k_B T \sum_{n=0}^{\infty} \ln\det[1 - \mathcal{S}_A(i\omega_n, \phi)\mathcal{S}_N(i\omega_n, \phi)], \quad (4)$$

where $\omega_n = (2n+1)\pi/\beta$ are Matsubara frequencies, while $\mathcal{S}_A$ and $\mathcal{S}_N$ are the scattering matrices of the junction for Andreev reflection and normal propagation, respectively (See Supplementary Material [49] for details). The Josephson current can be evaluated by $I(\phi) = \frac{2e}{\hbar}\frac{\partial F}{\partial \phi}$.

2.2 Energy-phase relation

At finite temperature, such as $k_B T = 0.15\Delta_{\rm sc}$, the dominant term in the Matsubara sum contributing to the free energy (Eq. (4)) is the ω_0 term. This leads to the expression for the Josephson current: $I(\phi) = \frac{2e}{\hbar}\big(-f_{\rm vp}\sin\phi + f_{\rm as}\cos\phi - 2f_2\sin 2\phi\big)$ [32, 49]. Here, the $\sin\phi$-term represents the conventional Josephson current originating from the tunneling of one Cooper pair during each tunneling event. The $\cos\phi$-term is the anomalous Josephson current caused by the finite phase difference between the two superconductors at the ground state [31]. The $\sin 2\phi$-term represents the second harmonic Josephson current originating from the tunneling of two pairs of Cooper pairs. The corresponding energy-phase relation $F(\phi)$ has the form of Eq. (1). To simplify the discussion, we define two energy scales: $E_T = \hbar v_f/d$ is the Thouless energy and $E_A = \hbar\delta v_f/d$ is the energy scale describing the intravalley inversion symmetry breaking, where $v_f^{-1} = \frac{1}{4}\sum_{\tau\alpha} v^{-1}_{{\rm vp},\tau\alpha}$, $\delta v_f^{-1} = \frac{1}{2}(v^{-1}_{{\rm vp},++} - v^{-1}_{{\rm vp},+-} + v^{-1}_{{\rm vp},--} - v^{-1}_{{\rm vp},-+})$. When the intravalley inversion asymmetry is small (for example, when λ_1 in Eq. (2) is small), E_A is large.

With the analytical form of the scattering matrices [49], we find that $f_{\rm vp} \propto \cos(\frac{2\Delta_{\rm vp}}{E_T})\cosh(\frac{\omega_0}{E_A})$ and $f_{\rm as} \propto \sinh(\frac{\omega_0}{E_A}) \times \sin(\frac{2\Delta_{\rm vp}}{E_T})$ by keeping ω_0 only. At $2\Delta_{\rm vp}/E_T = \pi/2 + m\pi$,

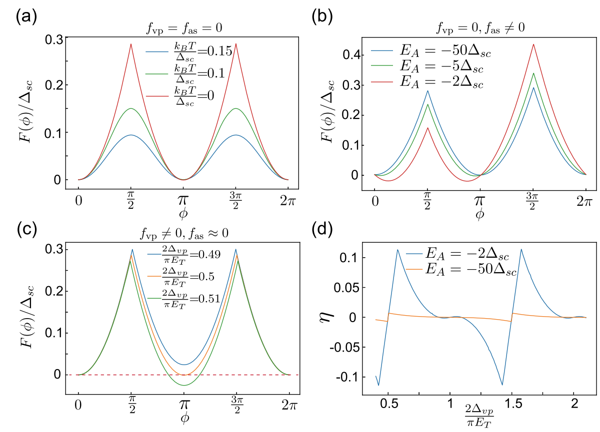

Figure 2 (a) Energy-phase relations at different temperatures with $E_A \gg \Delta_{\rm sc}$ and $2\Delta_{\rm vp}/E_T = \pi/2$. (b) Energy-phase relations for different E_A at zero temperature with $f_{\rm vp} = 0$ ($2\Delta_{\rm vp}/E_T = \pi/2$). (c) The $\Delta_{\rm vp}$ dependence of the energy-phase relation. As $2\Delta_{\rm vp}/E_T$ deviates from $\pi/2$, the degeneracy of the two local minima of the free energy is lifted. The results are obtained at zero temperature with $f_{\rm as} \approx 0$ ($E_A \gg \Delta_{\rm sc}$). (d) At zero temperature, the diode efficiency as a function of $2\Delta_{\rm vp}/\pi E_T$ for $E_A \simeq \Delta_{\rm sc}$ (transmon regime, blue line) and $E_A \gg \Delta_{\rm sc}$ (0-π qubit regime, orange line)

where m is an integer, we have $f_{\rm vp} = 0$. This reveals that the valley polarization is essential for suppressing the single Cooper pair tunnelling to achieve $f_{\rm vp} = 0$. The energy-phase relation $F(\phi)$ for $f_{\rm vp} = 0$ is shown in Fig. 2(b). Moreover, if $\Delta_{\rm sc}/E_A \ll 1$, then $f_{\rm as} \approx 0$ in Eq. (1), which can be achieved when E_A is large. If both of these two conditions are satisfied, the second harmonic term dominates $F(\phi)$ and a π-periodic Josephson junction can be realized. The $F(\phi)$ at different temperatures with both $f_{\rm vp} \approx f_{\rm as} \approx 0$ is shown in Fig. 2 (a). It is clear that there are energy minima at 0 and π phase of the junction. The $F(\phi)$ resembles the schematic illustration in Fig. 1 (d). In the following section we will show that this current-phase relation is desirable for realizing the 0-π qubit.

At low temperatures, the higher Matsubara frequencies are important but the π-periodicity of $F(\phi)$ is essentially the same as in the high temperature cases. On the other hand, if the intravalley inversion symmetry breaking is large (E_A is small), the $f_{\rm as}$ term can be significant. In this case, the $F(\phi)$ for different E_A is shown in Fig. 2(b). This case corresponds to the situation of Fig. 1 (e).

3 Results

3.1 0-π qubit

In this section, we construct the 0-π qubit by using the valley-polarized Josephson junction with $E_A \gg \Delta_{sc}$. As shown in Fig. 1 (a), the qubit consists of a valley-polarized Josephson junction shunted by a capacitor. The Hamiltonian of the qubit is

$$\hat{H}_{n_g} = 4E_C(\hat{n} - n_g)^2 + F(\hat{\phi}) \tag{5}$$

where $\hat{n}$ is the charge number operator, and n_g is the offset charge of the Josephson junction. $E_C = e^2/2C$ is the charging energy and $C = C_J + C_S$ is the total capacitance with C_J and C_S the capacitance of the Josephson junction and the shunted capacitor, respectively. The wave function $\psi(\phi)$ of qubit satisfies the boundary condition $\psi(\phi) = \psi(\phi + 2\pi)$. By making an analogy to the Bloch theorem, with $\hat{n}$, $-n_g$ and $\hat{\phi}$ playing the roles of momentum operator, crystal momentum and position operator, Eq. (5) can be seen as a particle moving in a periodic potential $F(\hat{\phi})$. Then we can solve charge dispersion, and denote it with $\epsilon(n_g)$, whose derivation is discussed in Supplementary [49]. The bandwidth of the dispersion reflects the sensitivity of the qubit to charge noise. Similar to the transmon case [18], we require the shunted capacitance to be large enough so that the bandwidth $\delta\epsilon$ [49] satisfies $\delta\epsilon/\epsilon \simeq \exp(-\int d\phi\sqrt{(F(\phi) - \epsilon)/4E_C}) \ll 1$, where ϵ is the energy level of qubit in the absence of n_g. For conventional transmons, this condition is reduced to $E_J/E_C \gg 1$ due to the simple form of its energy-phase relation $F(\phi) = -E_J\cos(\phi)$. Under this condition, the qubit is robust to charge noise.

As discussed above, for a valley-polarized Josephson junction with $2\Delta_{\rm vp}/E_T \approx \pi/2$, $F(\hat{\phi})$ is π-periodic as shown in Fig. 2 (a). At high temperature the energy-phase relation is dominated by the $\cos 2\phi$-term. As the temperature decreases, higher order terms also contribute to $F(\phi)$, with the $\cos 2m\phi$-terms becoming significant while still preserving the π-periodicity. When $2\Delta_{\rm vp}/E_T$ deviates from $\pi/2$, the degeneracy between the two local minima is lifted, resulting in a modified free energy, as shown in Fig. 2 (c). With a large E_A, which means that the intravalley inversion symmetry breaking term is negligible, the deviation of $2\Delta_{\rm vp}/\pi E_T$ from half integer induces an insignificant diode effect as shown in Fig. 2 (d). This indicates the 0-π qubit parameter regime of the junction. The energy and the wave functions of the qubit states for MATBG will be presented at the end of this work.

3.2 Transmon-like qubit

If the intravalley inversion symmetry of the valley-polarized weak link is significantly broken such that $E_A \simeq \Delta_{\rm sc}$, leading to a $\sin\phi$ term comparable to the $\cos 2\phi$ terms in the energy-phase relation. As shown in Fig. 2 (b) there are still two local minima within a period which are degenerate when $\Delta_{\rm vp}/E_T = \pi/4$, but the barrier at $\phi = 3\pi/2$ becomes much lower than that at $\phi = \pi/2$. Assuming there is no tunneling between the states at the two local minima of $F(\phi)$, the ground state and the first excited state energies are denoted as E_0 and E_1, respectively. With tunneling, the qubit states of the transmon qubit are the symmetric and antisymmetric linear combinations of the two states with energy E_0. Therefore, the qubit states are well separated from the higher energy states with energy in the order of E_1, resulting in a large anharmonicity [49]. Because $E_A \simeq \Delta_{sc}$, a remarkable diode effect can be observed when $2\Delta_{\rm vp}/\pi E_T$ deviates from half integer, which is shown in Fig. 2 (d).

3.3 Energy-phase relation of gate-defined Josephson junction of MATBG

In this section, we demonstrate the feasibility of realizing the energy-phase relation discussed in the previous sections in realistic gate-defined Josephson junctions of MATBG [31, 32]. The essential properties of moiré flat bands in MATBG can be captured by a tight binding model on a honeycomb lattice, yielding

$$\begin{aligned} H_0 = &\left[\sum_{\tau,\langle ij\rangle} t_1 c^{\dagger}_{i\tau}c_{j\tau} + \sum_{\tau,\langle ij\rangle'}(t_2 - i\tau t'_2)c^{\dagger}_{i\tau}c_{j\tau}\right] \\ &+ h.c. - \sum_{i,\tau}\mu c^{\dagger}_{i\tau}c_{i\tau}. \end{aligned} \tag{6}$$

Here, $\langle ij\rangle$ denotes the nearest hopping with amplitude t_1, while $\langle ij\rangle'$ sums over the fifth nearest hopping with amplitude t_2 and t'_2 [52, 53]. τ labels the two p-wave like orbital $p_x \pm i\tau p_y$, which represents the two valleys $\tau = \pm K$. The annihilation operator for an electron on site i with valley τ is denoted by $c_{i\tau}$. To demonstrate the 0-π qubit regime, we choose $t_1 = 4$ meV, $t_2 = 0.02$ meV and $t'_2 = 0$. Note that t'_2 represents the warping strength of the Fermi surface, which is set to be zero in this case. In our model, the superconducting region has the order parameter $\Delta_{\rm sc}$ and the weak link region has a valley polarization order parameter $\Delta_{\rm vp}$. The energy-phase relation of the 2D model can be obtained using the lattice Green's function method [49].

In Fig. 3 (a) we show the energy-phase relation of the 0-π qubit in MATBG with two different sets of parameters. This 0-π qubit is expected to be protected from decoherence originated from local perturbations [24–27]. Moreover, since only fully gapped superconductors are involved, we expect the quasiparticle poisoning-induced decoherence can be suppressed exponentially when the operating temperature scale is much smaller than the pairing gap $\Delta_{\rm sc}$.

On the other hand, for $t'_2 = 0.8$ meV, $t_1 = 4$ meV and $t_2 = 0.2$ meV with larger t_2 and t'_2, the energy-phase relation is shown in Fig. 3 (b), corresponding to the regime for valley-polarized Josephson junction. When the junction is shunted by a capacitor with $E_C = 2 \times 10^3$ MHz, the wave functions of the qubit states are displayed in Fig. 3 (b). The qubit state wave functions Ψ_{0S} and Ψ_{0AS}, which are the symmetric and the anti-symmetric terms with respect to ϕ, are well separated from the excited states Ψ_1 and Ψ_2

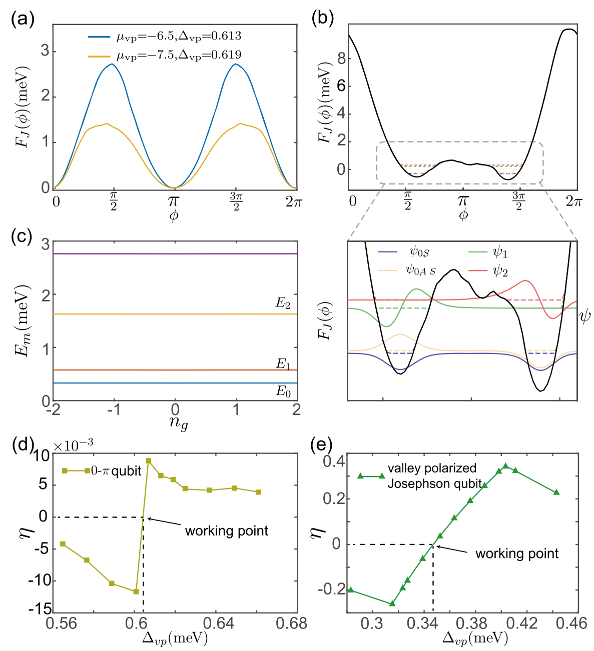

Figure 3 (a) Energy-phase relations in the 0-π qubit regime for two sets of parameters for the MATBG-based Josephson junction. The units for μ_{vp} and Δ_{vp} are meV, and set $\Delta_{sc} = 0.4$ meV. (b) Energy-phase relations for valley polarized Josephson junction in the transmon-like regime. Here, $\mu_{vp} = -7.5$ meV, $E_C = 2 \times 10^3$ MHz and $\Delta_{vp} = 0.363$ meV. The lower panel shows the wave function and the energy of the four lowest eigenstates of the corresponding qubit in the transmon-like regime. The energy levels of the four states are denoted by the horizontal dashed lines. (c) The first four eigenenergies E_m ($m = 0, 1, 2, 3$) as a function of offset charge n_g of a valley polarized MATBG Josephson qubit with charging energy $E_C = 0.2\Delta_{sc}$. (d)-(e) The nonreciprocity efficiency η as a function of Δ_{vp} in the neighbouring parameter regime of the working point. In (d) we set $t_2' = 5 \times 10^{-4} t_1$, and in (e) we set $t_2' = 0.2t_1$ with $t_1 = 4$ meV, while the diode is estimated at $T = 10$ mK

in energy. The energy splitting of the two-qubit states is $0.01E_C$ and the energy gap between the qubit states and the excited states is approximately $60E_C$. These energy levels labeled by the horizontal dashed lines in Fig. 3 (b) exhibit remarkable stability against perturbations in n_g [Fig. 3 (c)], resulting in long decoherence time against charge fluctuations [49].

These two kinds of qubit design can be distinguished by nonreciprocity efficiency η around the working point. For the 0-π qubit, where the trigonal warping term is tiny and the free energy functional is approximately $F(\phi) = \cos 2\phi$, η remains small with $\eta < 0.02$ around the working point, and vanishes when the system is sitting exactly at the working point [see Fig. 3 (d)]. On the other hand, for the valley polarized Josephson junction, a vanishing η indicates the desired energy phase relation. In contrast to the 0-π qubit case, when the parameter deviates slightly from the $\eta = 0$ point, a very large $\eta \approx 0.3$ is observed, indicating a large diode effect shows up in the system [see Fig. 3 (e)]. This is compatible with the results from 1D analytic calculation [see Fig. 2 (d)], and could be regarded as a criterion to distinguish between these two kinds of qubit designs.

4 Discussion

Recently, qubit realizations using a single Josephson junction with unconventional energy-phase relation have attracted much attention [54–56]. In particular, at the concluding stage of this work, we came across proposals using d-wave superconductors to construct Josephson junctions with unconventional energy-phase relations [55, 56]. On the other hand, the proposed gate-defined MATBG-based qubits do not require external magnetic fields nor unconventional superconductors. Importantly, the proposed Josephson junction had been experimentally realized [30]. In addition, the gatemons, based on semiconductor nanowires [57–59] are also transmon-like qubits which can be manipulated through electrostatic gating. However, there is no unconventional energy-phase relation in gatemons and they are not related to the 0-π qubits discussed in this work.

Supplementary information

Supplementary information accompanies this paper at https://doi.org/10.1007/s44214-026-00100-3.

Additional file 1. (PDF 6.4 MB)

Acknowledgements

K.T.L. acknowledges the support of the Ministry of Science and Technology, China, and the Hong Kong Research Grants Council through Grants No. 2020YFA0309600, No. RFS2021-6S03, No. C6025-19G, No. AoE/P-701/20, No. 16310520, No. 16310219 and No. 16307622.

Author contributions

KTL supervised the project. YX and ZCF carried out the analytical and numerical calculations. YX, ZCF, ZT, JX, and KTL discussed the results and contributed to the writing of the manuscript. All authors read and approved the final manuscript.

Availability of data and material

The data used and analysed during the current study are available from the corresponding author on reasonable request.

Declarations

Competing interests

Author K. T. Law is a member of the Editorial Board of *Quantum Frontiers*. This author was excluded from the editorial handling and peer review process for this manuscript. All other authors declare no competing interests.

Received: 26 November 2025 Revised: 22 January 2026
Accepted: 10 February 2026 Published online: 25 February 2026

References

1. J.-Q. You, F. Nori, Atomic physics and quantum optics using superconducting circuits. Nature **474**(7353), 589–597 (2011). https://doi.org/10.1038/nature10122

2. A.A. Houck, H.E. Türeci, J. Koch, On-chip quantum simulation with superconducting circuits. Nat. Phys. **8**(4), 292–299 (2012). https://doi.org/10.1038/nphys2251
3. X. Tan, D.-W. Zhang, Z. Yang, J. Chu, Y.-Q. Zhu, D. Li, X. Yang, S. Song, Z. Han, Z. Li, Y. Dong, H.-F. Yu, H. Yan, S.-L. Zhu, Y. Yu, Experimental measurement of the quantum metric tensor and related topological phase transition with a superconducting qubit. Phys. Rev. Lett. **122**, 210401 (2019). https://doi.org/10.1103/PhysRevLett.122.210401
4. Y. Makhlin, G. Schön, A. Shnirman, Quantum-state engineering with Josephson-junction devices. Rev. Mod. Phys. **73**, 357–400 (2001). https://doi.org/10.1103/RevModPhys.73.357
5. H.J. Kimble, The quantum internet. Nature **453**(7198), 1023–1030 (2008). https://doi.org/10.1038/nature07127
6. J.M. Gambetta, J.M. Chow, M. Steffen, Building logical qubits in a superconducting quantum computing system. npj Quantum Inf. **3**(1), 2 (2017). https://doi.org/10.1038/s41534-016-0004-0
7. P. Krantz, M. Kjaergaard, F. Yan, T.P. Orlando, S. Gustavsson, W.D. Oliver, A quantum engineer's guide to superconducting qubits. Appl. Phys. Rev. **6**(2) (2019). https://doi.org/10.1063/1.5089550
8. Google AI Quantum and Collaborators, Hartree-Fock on a superconducting qubit quantum computer. Science **369**(6507), 1084–1089 (2020). https://doi.org/10.1126/science.abb9811
9. M. Kjaergaard, M.E. Schwartz, J. Braumüller, P. Krantz, J.I.-J. Wang, S. Gustavsson, W.D. Oliver, Superconducting qubits: current state of play. Annu. Rev. Condens. Matter Phys. **11**(1), 369–395 (2020). https://doi.org/10.1146/annurev-conmatphys-031119-050605
10. U. Vool, M. Devoret, Introduction to quantum electromagnetic circuits. Int. J. Circuit Theory Appl. **45**(7), 897–934 (2017). https://doi.org/10.1002/cta.2359
11. S.E. Rasmussen, K.S. Christensen, S.P. Pedersen, L.B. Kristensen, T. Bækkegaard, N.J.S. Loft, N.T. Zinner, Superconducting circuit companion—an introduction with worked examples. PRX Quantum **2**, 040204 (2021). https://doi.org/10.1103/PRXQuantum.2.040204
12. B.D. Josephson, The discovery of tunnelling supercurrents. Rev. Mod. Phys. **46**, 251–254 (1974). https://doi.org/10.1103/RevModPhys.46.251
13. M.H. Devoret, A. Wallraff, J.M. Martinis, *Superconducting Qubits: A Short Review* (2004)
14. J.Q. You, F. Nori, Superconducting circuits and quantum information. Phys. Today **58**(11), 42–47 (2005). https://doi.org/10.1063/1.2155757. Accessed 2023-09-11
15. V. Bouchiat, D. Vion, P. Joyez, D. Esteve, M. Devoret, Quantum coherence with a single Cooper pair. Phys. Scr. **1998**(T76), 165 (1998). https://doi.org/10.1238/Physica.Topical.076a00165
16. Y. Nakamura, Y.A. Pashkin, J. Tsai, Coherent control of macroscopic quantum states in a single-Cooper-pair box. Nature **398**(6730), 786–788 (1999). https://doi.org/10.1038/19718
17. A. Blais, A.L. Grimsmo, S.M. Girvin, A. Wallraff, Circuit quantum electrodynamics. Rev. Mod. Phys. **93**, 025005 (2021). https://doi.org/10.1103/RevModPhys.93.025005
18. J. Koch, T.M. Yu, J. Gambetta, A.A. Houck, D.I. Schuster, J. Majer, A. Blais, M.H. Devoret, S.M. Girvin, R.J. Schoelkopf, Charge-insensitive qubit design derived from the Cooper pair box. Phys. Rev. A **76**, 042319 (2007). https://doi.org/10.1103/PhysRevA.76.042319
19. J.A. Schreier, A.A. Houck, J. Koch, D.I. Schuster, B.R. Johnson, J.M. Chow, J.M. Gambetta, J. Majer, L. Frunzio, M.H. Devoret, S.M. Girvin, R.J. Schoelkopf, Suppressing charge noise decoherence in superconducting charge qubits. Phys. Rev. B **77**, 180502 (2008). https://doi.org/10.1103/PhysRevB.77.180502
20. J. Mooij, T. Orlando, L. Levitov, L. Tian, C.H. Wal, S. Lloyd, Josephson persistent-current qubit. Science **285**(5430), 1036–1039 (1999). https://doi.org/10.1126/science.285.5430.1036
21. T.P. Orlando, J.E. Mooij, L. Tian, C.H. Wal, L.S. Levitov, S. Lloyd, J.J. Mazo, Superconducting persistent-current qubit. Phys. Rev. B **60**, 15398–15413 (1999). https://doi.org/10.1103/PhysRevB.60.15398
22. J.Q. You, X. Hu, S. Ashhab, F. Nori, Low-decoherence flux qubit. Phys. Rev. B **75**, 140515 (2007). https://doi.org/10.1103/PhysRevB.75.140515
23. F. Yan, S. Gustavsson, A. Kamal, J. Birenbaum, A.P. Sears, D. Hover, T.J. Gudmundsen, D. Rosenberg, G. Samach, S. Weber, et al., The flux qubit revisited to enhance coherence and reproducibility. Nat. Commun. **7**(1), 12964 (2016). https://doi.org/10.1038/ncomms12964
24. A. Kitaev, Protected qubit based on a superconducting current mirror (2006). https://doi.org/10.48550/arXiv.cond-mat/0609441
25. P. Brooks, A. Kitaev, J. Preskill, Protected gates for superconducting qubits. Phys. Rev. A **87**, 052306 (2013). https://doi.org/10.1103/PhysRevA.87.052306
26. J.M. Dempster, B. Fu, D.G. Ferguson, D.I. Schuster, J. Koch, Understanding degenerate ground states of a protected quantum circuit in the presence of disorder. Phys. Rev. B **90**, 094518 (2014). https://doi.org/10.1103/PhysRevB.90.094518
27. P. Groszkowski, A.D. Paolo, A. Grimsmo, A. Blais, D. Schuster, A.A. Houck, J. Koch, Coherence properties of the 0-π qubit. New J. Phys. **20**(4), 043053 (2018). https://doi.org/10.1088/1367-2630/aab7cd
28. C. Schrade, C.M. Marcus, A. Gyenis, Protected hybrid superconducting qubit in an array of gate-tunable Josephson interferometers. PRX Quantum **3**, 030303 (2022). https://doi.org/10.1103/PRXQuantum.3.030303
29. A. Gyenis, P.S. Mundada, A. Di Paolo, T.M. Hazard, X. You, D.I. Schuster, J. Koch, A. Blais, A.A. Houck, Experimental realization of a protected superconducting circuit derived from the 0–π qubit. PRX Quantum **2**, 010339 (2021). https://doi.org/10.1103/PRXQuantum.2.010339
30. J. Díez-Mérida, A. Díez-Carlón, S.Y. Yang, Y.-M. Xie, X.-J. Gao, J. Senior, K. Watanabe, T. Taniguchi, X. Lu, A.P. Higginbotham, K.T. Law, D.K. Efetov, Symmetry-broken Josephson junctions and superconducting diodes in magic-angle twisted bilayer graphene. Nat. Commun. **14**, 2396 (2023). https://doi.org/10.1038/s41467-023-38005-7
31. Y.-M. Xie, D.K. Efetov, K.T. Law, φ_0-Josephson junction in twisted bilayer graphene induced by a valley-polarized state. Phys. Rev. Res. **5**, 023029 (2023). https://doi.org/10.1103/PhysRevResearch.5.023029
32. J.-X. Hu, Z.-T. Sun, Y.-M. Xie, K.T. Law, Josephson diode effect induced by valley polarization in twisted bilayer graphene. Phys. Rev. Lett. **130**, 266003 (2023). https://doi.org/10.1103/PhysRevLett.130.266003
33. H.C. Po, L. Zou, A. Vishwanath, T. Senthil, Origin of Mott insulating behavior and superconductivity in twisted bilayer graphene. Phys. Rev. X **8**, 031089 (2018). https://doi.org/10.1103/PhysRevX.8.031089
34. F. Ando, Y. Miyasaka, T. Li, J. Ishizuka, T. Arakawa, Y. Shiota, T. Moriyama, Y. Yanase, T. Ono, Observation of superconducting diode effect. Nature **584**(7821), 373–376 (2020). https://doi.org/10.1038/s41586-020-2590-4
35. M. Davydova, S. Prembabu, L. Fu, Universal Josephson diode effect. Sci. Adv. **8**(23), 0309 (2022). https://doi.org/10.1126/sciadv.abo0309. Accessed 2023-09-11
36. J.-X. Lin, P. Siriviboon, H.D. Scammell, S. Liu, D. Rhodes, K. Watanabe, T. Taniguchi, J. Hone, M.S. Scheurer, J. Li, Zero-field superconducting diode effect in small-twist-angle trilayer graphene. Nat. Phys. **18**(10), 1221–1227 (2022). https://doi.org/10.1038/s41567-022-01700-1
37. H. Wu, Y. Wang, Y. Xu, P.K. Sivakumar, C. Pasco, U. Filippozzi, S.S. Parkin, Y.-J. Zeng, T. McQueen, M.N. Ali, The field-free Josephson diode in a van der Waals heterostructure. Nature **604**(7907), 653–656 (2022). https://doi.org/10.1038/s41586-022-04504-8
38. Y. Zhang, Y. Gu, P. Li, J. Hu, K. Jiang, General theory of Josephson diodes. Phys. Rev. X **12**, 041013 (2022). https://doi.org/10.1103/PhysRevX.12.041013
39. A. Daido, Y. Ikeda, Y. Yanase, Intrinsic superconducting diode effect. Phys. Rev. Lett. **128**, 037001 (2022). https://doi.org/10.1103/PhysRevLett.128.037001
40. A. Daido, Y. Yanase, Superconducting diode effect and nonreciprocal transition lines. Phys. Rev. B **106**, 205206 (2022). https://doi.org/10.1103/PhysRevB.106.205206
41. B. Pal, A. Chakraborty, P.K. Sivakumar, M. Davydova, A.K. Gopi, A.K. Pandeya, J.A. Krieger, Y. Zhang, M. Date, S. Ju, et al., Josephson diode effect from Cooper pair momentum in a topological semimetal. Nat. Phys. **18**(10), 1228–1233 (2022). https://doi.org/10.1038/s41567-022-01699-5
42. Y. Tanaka, B. Lu, N. Nagaosa, Theory of giant diode effect in *d*-wave superconductor junctions on the surface of a topological insulator. Phys. Rev. B **106**, 214524 (2022). https://doi.org/10.1103/PhysRevB.106.214524
43. R.S. Souto, M. Leijnse, C. Schrade, Josephson diode effect in supercurrent interferometers. Phys. Rev. Lett. **129**, 267702 (2022). https://doi.org/10.1103/PhysRevLett.129.267702
44. J.J. He, Y. Tanaka, N. Nagaosa, A phenomenological theory of superconductor diodes. New J. Phys. **24**(5), 053014 (2022). https://doi.org/10.1088/1367-2630/ac6766
45. S. Ilić, F.S. Bergeret, Theory of the supercurrent diode effect in Rashba superconductors with arbitrary disorder. Phys. Rev. Lett. **128**, 177001 (2022). https://doi.org/10.1103/PhysRevLett.128.177001

46. C. Ciaccia, R. Haller, A.C.C. Drachmann, T. Lindemann, M.J. Manfra, C. Schrade, C. Schönenberger, Gate-tunable Josephson diode in proximitized inas supercurrent interferometers. Phys. Rev. Res. **5**, 033131 (2023). https://doi.org/10.1103/PhysRevResearch.5.033131
47. B. Lu, S. Ikegaya, P. Burset, Y. Tanaka, N. Nagaosa, Tunable Josephson diode effect on the surface of topological insulators. Phys. Rev. Lett. **131**, 096001 (2023). https://doi.org/10.1103/PhysRevLett.131.096001
48. C. Beenakker, Three "universal" mesoscopic Josephson effects, in *Transport Phenomena in Mesoscopic Systems: Proceedings of the 14th Taniguchi Symposium, Shima, Japan, November 10–14, 1991* (Springer, Berlin, 1992), pp. 235–253. https://doi.org/10.1007/978-3-642-84818-6_22
49. See Supplementary Material for: (i) analytical model of valley polarized Josephson junction, (ii) tight binding model and numerical calculation, (iii) qubit design and coherence properties
50. A. Furusaki, Dc Josephson effect in dirty sns junctions: numerical study. Physica B, Condens. Matter **203**(3), 214–218 (1994). https://doi.org/10.1016/0921-4526(94)90061-2
51. P. Brouwer, C. Beenakker, Anomalous temperature dependence of the supercurrent through a chaotic Josephson junction. Chaos Solitons Fractals **8**(7–8), 1249–1260 (1997). https://doi.org/10.1016/S0960-0779(97)00018-0
52. M. Koshino, N.F.Q. Yuan, T. Koretsune, M. Ochi, K. Kuroki, L. Fu, Maximally localized Wannier orbitals and the extended Hubbard model for twisted bilayer graphene. Phys. Rev. X **8**, 031087 (2018). https://doi.org/10.1103/PhysRevX.8.031087
53. N.F.Q. Yuan, L. Fu, Model for the metal-insulator transition in graphene superlattices and beyond. Phys. Rev. B **98**, 045103 (2018). https://doi.org/10.1103/PhysRevB.98.045103
54. G.-L. Guo, H.-B. Leng, Y. Hu, X. Liu, 0–π qubit with one Josephson junction. Phys. Rev. B **105**, 180502 (2022). https://doi.org/10.1103/PhysRevB.105.L180502
55. H. Patel, V. Pathak, O. Can, A.C. Potter, M. Franz, d-mon: a transmon with strong anharmonicity based on planar c-axis tunneling junction between d-wave and s-wave superconductors. Phys. Rev. Lett. **132**(1), 017002 (2024). https://doi.org/10.1103/PhysRevLett.132.017002
56. V. Brosco, G. Serpico, V. Vinokur, N. Poccia, U. Vool, Superconducting qubit based on twisted cuprate van der Waals heterostructures. Phys. Rev. Lett. **132**(1), 017003 (2024). https://doi.org/10.1103/PhysRevLett.132.017003
57. T.W. Larsen, K.D. Petersson, F. Kuemmeth, T.S. Jespersen, P. Krogstrup, J. Nygård, C.M. Marcus, Semiconductor-nanowire-based superconducting qubit. Phys. Rev. Lett. **115**, 127001 (2015). https://doi.org/10.1103/PhysRevLett.115.127001
58. A. Hertel, M. Eichinger, L.O. Andersen, D.M.T. Zanten, S. Kallatt, P. Scarlino, A. Kringhøj, J.M. Chavez-Garcia, G.C. Gardner, S. Gronin, M.J. Manfra, A. Gyenis, M. Kjaergaard, C.M. Marcus, K.D. Petersson, Gate-tunable transmon using selective-area-grown superconductor-semiconductor hybrid structures on silicon. Phys. Rev. Appl. **18**, 034042 (2022). https://doi.org/10.1103/PhysRevApplied.18.034042
59. A. Danilenko, D. Sabonis, G.W. Winkler, O. Erlandsson, P. Krogstrup, C.M. Marcus, Few-mode to mesoscopic junctions in gatemon qubits. Phys. Rev. B **108**, 020505 (2023). https://doi.org/10.1103/PhysRevB.108.L020505

Publisher's note